Applied Catalysis A: General 482 (2014) 352–361

Contents lists available at ScienceDirect

Applied Catalysis A: General

journal homepage: www.elsevier.com/locate/apcata

Hydrodeoxygenation of m-cresol with Pt supported over mild acid materials

M.S. Zanuttini, B.O. Dalla Costa, C.A. Querini*, M.A. Peralta

Research Institute on Catalysis and Petrochemistry (INCAPE), (FIQ-UNL, CONICET), Santiago del Estero 2654, S3000AOJ Santa Fe, Argentina

ARTICLE INFO

Article history:
Received 18 April 2014
Received in revised form 8 June 2014
Accepted 14 June 2014
Available online 20 June 2014

Keywords:
Hydrodeoxygenation
Cresol
Beta zeolite
Alumina
Silica
Platinum

ABSTRACT

The deoxygenation of m-cresol was studied using Pt catalysts supported on different materials of various levels of acidity, such as gamma alumina, silica, and H-BEA zeolites. The reaction was carried out at atmospheric pressure and 300 °C in a fixed-bed reactor. The catalysts were characterized by XRD, BET, TPR, TEM, H_2 and CO chemisorptions, pyridine-TPD and pyridine-IR. The (metal function/acid function) ratio and the reaction conditions were adjusted in order to have a high selectivity to toluene. The effects of acid sites density, strength and type, as well as the pore structure of the different supports on the deoxygenation activity, selectivity and stability were addressed. In order to avoid the production of heavy products and a fast deactivation, the concentration of Brønsted acid sites must be very low. A high acid sites density is detrimental for catalyst stability, due to coke formation via condensation of precursors adsorbed on adjacent sites. Additionally, a mesoporous structure is better than a microporous structure regarding the stability. All the catalysts can be regenerated in air at relatively low temperature.

1. Introduction

Biomass fast pyrolysis is a process in which a product called bio-oil is obtained, which is used both as an energy source and a feedstock for chemical production. Bio-oil is a complex mixture of acids, alcohols, aldehydes, esters, ketones, phenols, guaiacols, syringols, sugars, furans, alkenes, aromatics, nitrogen compounds, and miscellaneous oxygenates [1,2]. In contrast to petroleum fuels, bio-oil contains a large amount of oxygen, usually 45–50%. Thus, its elemental composition resembles more to the biomass from which it was derived than to the petroleum oils. For example, wood can be approximately represented by the formula $CH_{1.4}O_{0.6}$, i.e. it contains 42 wt% of oxygen. This oxygen is present in most of the more than 300 compounds that have been identified in the bio-oils [3]. The presence of oxygen is the primary reason for the difference in the properties and behaviour between hydrocarbon fuels and bio-oils [4]. Although the pyrolysis liquid is called "bio-oil", it is immiscible with liquid hydrocarbons, because of its high polarity and hydrophilic nature. Even though it is a potential fuel, it cannot be used as such without prior refining due to its high viscosity, low heating value, corrosiveness and instability [5,6]. The refining essentially involves the removal of oxygen, since it imparts to this biofuel the undesirable properties mentioned above [7]. Phenolic compounds represent an important fraction of the bio-oil. The studies of deoxygenation reactions using model compounds with different types of catalysts showed that either the phenolic fraction was not deoxygenated, or it was deoxygenated but using a high hydrogen consumption and high pressure. Besides, when using high hydrogen pressures, the formation of fully hydrogenated products of lower octane number and therefore, less important in order to be fed to the fuel pool, was generally observed. Several catalysts, mostly hydrotreating catalysts, were used to deoxygenate phenolic compounds at high hydrogen pressures. Some examples are unsupported MoS_2 and $CoMoS_2$ [8], Co-Mo-B [9], $NiMoP/Al_2O_3$ [10], $CoO\text{-}MoO_3/Al_2O_3$ [11], $MoO_3\text{-}NiO/Al_2O_3$ [12], $Rh/SiO_2\text{-}Al_2O_3$ and $Ru/SiO_2\text{-}Al_2O_3$ [13], NiMo sulphide [14], MoS_2/Al_2O_3 and $CoMoS/Al_2O_3$ [15], $Ni,Mo/Al_2O_3$, Mo/Al_2O_3 and $Co,Mo/Al_2O_3$ [16] and CoMoS [17]. There are few reports in which good results were presented, related to the deoxygenation of these compounds with low hydrogen consumption at atmospheric pressure and high selectivities to high octane deoxygenated aromatics. For example, phenol was deoxygenated with high selectivity to benzene, at atmospheric pressure with Ni/SiO_2 catalyst [18] and cresol was deoxygenated to toluene, benzene and xylene, also at atmospheric pressure with the Ga/HBeta catalyst [19]. Resasco et al. [20] investigated the deoxygenation of anisole, comparing the performance of the HBeta zeolite and Pt/HBeta. In the bifunctional catalyst, methyl transference and hydrodeoxygenation reactions occurred at higher speeds than in the monofunctional catalysts. Moreover, in Pt/HBeta catalyst deactivation rate and coke deposition was

* Corresponding author. Tel.: +54 342 4533858; fax: +54 342 4531068.
E-mail address: querini@fiq.unl.edu.ar (C.A. Querini).

http://dx.doi.org/10.1016/j.apcata.2014.06.015
0926-860X/

reduced compared with the zeolite. On the other hand, results obtained in the deoxygenation of phenol, 2-metoxi-4-(2-propenil) phenol and other phenolic compounds using HZSM-5 catalysts were not satisfactory [21–23]. The Fe/SiO_2 catalyst [24] was used to deoxygenate guaiacol. This compound was also deoxygenated with Pt–Sn [25] and V_2O_5/Al_2O_3 catalysts [26], but phenol was the main product in both cases.

In this work, the deoxygenation at atmospheric pressure of m-cresol, taken as a model compound of the bio-oil phenolic fraction, was studied using Pt supported on different materials. The use of solid acid catalysts is particularly attractive because several of the biomass deoxygenation reactions take place through decarbonylation, decarboxylation and dehydration followed by oligomerization of olefins, as well as many other reactions such as cyclization, hydrogen transfer, alkylation and cracking. Usually, a complex mixture of hydrocarbons in the gasoline range (besides some shorter compounds such as methane, ethylene, etc.), including substantial amounts of aromatics, is obtained without the concomitant consumption of hydrogen occurring on supported metal catalysts. However, as above mentioned, the deoxygenation of phenolic compounds requires the use of metallic catalysts. In previous works [27], the deoxygenation of a phenolic compound (m-cresol) with Pt supported on gamma alumina was studied. Toluene, benzene and methylcyclohexane were the main reaction products. It was shown that the yield of the desired product can be regulated by changing the metal loading, the H_2/cresol ratio and the reaction temperature. The toluene hydrogenation to methylcyclohexane was favoured at low temperature, while the toluene yield has a maximum at an intermediate temperature level (around 300 °C), since at high temperatures toluene was transformed into benzene by demethylation. The metal loading has a strong influence in the product distribution, because as the ratio of metal/acid sites increased, the toluene formation was favoured. It has been proposed that a direct hydrogenolysis of the $C_{aromatic}$—OH bond cannot occur [20]. The apparent direct hydrodeoxygenation may involve a partial hydrogenation of the phenolic ring near the $C_{aromatic}$—OH bond, resulting in the temporary removal of the delocalization effect, followed by rapid dehydration and a consecutive dehydrogenation.

In order to study the effect of the acidity required for cresol deoxygenation, different supports were studied. Among them, supports with very low acidity such as gamma alumina and silica gel were included, and also the mild-acid supports H-BEA, and H-BEA modified with lanthanum and sodium by ion exchange. The effect of the surface structure was also analyzed.

2. Experimental

2.1. Catalysts preparation

The catalysts were prepared by wet impregnation of tetramine platinum (II) nitrate (metal content 50 wt%) supplied by Alfa Aesar. An aqueous solution of 1 wt% of $Pt(NH_3)_4(NO_2)_3$ was used to prepare the Pt catalysts. The preparation procedure was the same for all the catalysts, achieving a platinum loading of 1.7 wt%. A suspension of the support in the metal precursor solution was stirred on a hot plate at 110 °C until complete evaporation. The impregnated catalyst was dried in an oven at 110 °C for 12 h. The dried sample was calcined in an electric furnace at 350 °C for 2 h. The supports used were γ-Al_2O_3 (CK-300, Ketjen), SiO_2 gel (Alfa Aesar) and H-BEA zeolites from UOP, Si/Al = 13. This support was labelled H-B. This zeolite was exchanged with a $La(NO_3)_3$ 0.5 M aqueous solution, during 3 h in reflux. Then it was filtered and dried at 100 °C, and finally calcined at 550 °C. This material was used for a second ionic exchange with NH_4NO_3 0.5 M during 3 h in reflux, drying and calcining at 550 °C. The final content of La in this case was 0.03 wt%. This support was labelled LCH-B. A similar procedure was followed to prepare another catalyst, LCL-B, using $La(NO_3)_3$ also in the second ion exchange, reaching a lanthanum content of 4.2 wt%. Finally, H-B zeolite was exchanged with a solution of NaOH 0.25 M for 3 h in reflux. Afterwards, it was filtered and dried at 100 °C, and then calcined at 550 °C. The sodium content of this zeolite was 1 wt%. This support was labelled Na-B. The chemicals used for the ionic exchange were $La(NO_3)_3{\cdot}6H_2O$ (Merck), NH_4NO_3 (Anedra) and NaOH (Ciccarelli). Na-B catalyst was exchanged with NH_4NO_3 in order to go back to the original protonic form, and compare with the sodic form, and also to verify if there was a structural change during these ion-exchange steps, mainly during the contact with the NaOH solution. This support was labelled NaH-B.

2.2. Catalysts characterization

Nitrogen adsorption was employed to determine BET surface areas and pores volumes, using a Quantachrome Autosorb 1 analyzer. Micropores volumes were estimated by means of *t*-plots and Saito-Foley method was used to estimate the average micropore sizes. The determinations were carried out by pre-treating the catalysts under vacuum at 350 °C for 3 h. The mesopores volumes were calculated as the difference between the total pores volumes and the micropores volumes.

Catalysts crystalline structures were characterized by X-ray Diffraction (XRD). The X-ray diffractograms were obtained with a Shimadzu XD-D1 instrument with monochromator using CuK_α radiation (30 kV, 40 mA) at a scanning rate of $4^\circ\,min^{-1}$ for Pt/γ-Al_2O_3 and Pt/SiO_2 catalysts, and at $0.5^\circ\,min^{-1}$ for Pt/zeolites catalysts, from $2\theta = 5–100^\circ$. The crystallite size of Pt, determined as the thickness of crystal in a direction perpendicular to the (1 1 1) lattice plane (*Lc*) was determined by the following Scherrer's equation:

$$Lc = \frac{K\lambda}{\beta \cos\theta} \quad (1)$$

where, β is the full width at half maximum (FWHM) in radian, λ is the X-ray wavelength (0.154 nm), θ is the Bragg angle, and K is the Scherrer's constant equal to 0.9.

The metallic particles size for Pt/γ-Al_2O_3 and Pt/SiO_2 catalysts were determined by Transmission Electron Microscopy (TEM). The reduced samples were dispersed in distilled water, and then one drop of this suspension was placed on holey carbon supported on a copper grid. The micrograph images of the samples were acquired with a JEOL 100 CX model microscope at 100 kV, and a magnification of 450,000×.

Reducibility of metallic catalysts was studied by Temperature-Programmed Reduction (TPR) analysis using a TCD detector. The gas mixture was 5% H_2 in Ar. The temperature was increased from 20 to 700 °C with a heating rate of 11 °C min^{-1}.

The metallic dispersions were determined both by H_2 and CO chemisorption. The H_2 chemisorption measurements were made in volumetric equipment at room temperature. Each sample was outgassed under vacuum (10^{-4} Torr). The adsorption isotherms were measured at room temperature between 25 and 100 Torr. In this range of pressure the isotherms were linear, and the H_2 chemisorption capacity was calculated by extrapolation of the isotherms to zero pressure [28]. The CO chemisorption experiments were carried out in a fixed bed reactor. The sample were reduced with H_2 and then purged with N_2 to desorb any hydrogen remaining on the metal. After this treatment, pulses of 250 μl of 2.5% CO in Ar were sent to the catalyst at room temperature. The gas coming out of the cell was fed to a methanation reactor, in order to increase the system sensitivity. In this reactor, CO

reacts with H_2 over a Ni catalyst producing CH_4, which is fed to a flame ionization detector (FID). For dispersion calculations a 1:1 stoichiometry for the CO chemisorption on the metal atoms was assumed.

The acidity of the samples was studied by two techniques. In the Pyridine-Temperature-Programmed Desorption (Py-TPD) technique, the catalysts were pretreated in situ in N_2 flow at 350 °C for 1 h. After cooling down to room temperature, the sample was saturated with pyridine. After this, pure nitrogen was flowed and the temperature was increased up to 150 °C, until no pyridine was detected in the gas coming out of the cell. The TPD experiment was carried out heating at 12 °C min^{-1}, from 150 to 750 °C. Pyridine was detected using a FID detector after methanation.

Using the values of metallic dispersion determined by CO and H_2 chemisorptions it was possible to obtain the number of exposed Pt atoms (MS), while the number of acid sites was measured by Py-TPD (AS). With these two values, the ratio (number of metallic sites/number of acid sites) was calculated (MS/AS).

The amount of Brønsted and Lewis acid sites was determined by FTIR analyses of pyridine adsorbed on the samples (Py-IR). Spectral measurements were performed on a JASCO FT-IR 5300 spectrometer equipped with a DTGS detector. The range and resolution of acquisition were 4600–400 and 4 cm^{-1} respectively. A self-supporting wafer for each sample (~20 mg and 13 mm of diameter) was prepared, placed in a thermostated cell with CaF_2 windows connected to a vacuum line, and evacuated for 8 h at 400 °C. The background spectrum was recorded after cooling the sample to room temperature. Afterwards, the solid wafer was exposed to pyridine vapours (Sintorgan, 99% purity) until the system was saturated to 46 mmHg at room temperature; the contact time at this pressure was 12 h. The IR spectrum for each sample was obtained after pyridine desorption by evacuation for 1 h at 250, 350 and 400 °C. All the spectra were recorded at room temperature after pyridine desorption at each temperature. The difference spectrum was finally obtained by subtracting the background spectrum previously recorded.

The amount of carbonaceous materials deposited on the spent catalysts were determined by Temperature-Programmed Oxidation (TPO), using a stream of 5% O_2 in N_2 and a heating rate of 12 °C min^{-1}. The oxidation products were detected with a FID detector after methanation.

2.3. Catalytic activity

The catalytic activity was measured at atmospheric pressure in a continuous fixed-bed reactor, made of 5 mm internal diameter quartz tube. The catalyst bed was supported with quartz wool. Above the catalytic bed, quartz beads were loaded in order to improve the heat transfer. The catalyst was pretreated under flow of H_2 (30 ml min^{-1}) by heating at 10 °C min^{-1} from room temperature to 500 °C and kept at this temperature for 1 h. Then it was cooled to the reaction temperature (300 °C). The carrier was bubbled in liquid m-cresol maintained at a preselected temperature in the range 55–90 °C, in order to saturate the gas. The carrier flow rate was 5–16 ml min^{-1}. Under these conditions the cresol partial pressure in the gas stream fed to the reactor was between 1.5 and 11.7 Torr, and the residence time (W/F) was between 0.08 and 11 g_{cat} h $g_{cresol}{}^{-1}$. After each run, the catalyst bed was purged with H_2 at the reaction temperature for 30 min. The gas flow rates were controlled with mass flow controllers (Aalborg Instruments and Controls, Inc.). The reactor outlet stream was analyzed in a GC (SRI 8610) connected online and equipped with a ZB-5 capillary column (15 m) and FID detector. A split ratio of 100 was used. Standard samples were used in order to identify the reaction products. In addition, a GC–MS (Varian Saturn 2000) equipped with a HP-5 capillary column was used to identify the reaction products collected in a condenser cooled at 0 °C. The non-condensed gases were analyzed by GC using a Petrocol (Supelco) capillary column (100 m).

Products selectivity (S) and cresol conversion (X) were calculated according to the following equations:

$$Am_i = \frac{A_i}{f_i\, MW_i} \tag{2}$$

$$y_i = \frac{Am_i}{\sum_{i=1}^{n} Am_i} \tag{3}$$

$$S_i(\%) = \frac{y_i/\nu_i}{\sum_{i=2}^{n}(y_i/\nu_i)}100 \tag{4}$$

$$X(\%) = \frac{\sum_{i=2}^{n} y_i/\nu_i}{\sum_{i=1}^{n} y_i/\nu_i}100 \tag{5}$$

where Am_i is the area obtained in the chromatogram for compound i, f_i: response factor for compound i, MW_i: molecular weight, y_i: yield of compound i, and ν_i is a coefficient which represents the number of moles of a given product i obtained per mole of cresol ($i = 1$).

Catalyst regeneration was carried out after reactions at W/F = 0.08 g_{cat} h $g_{cresol}{}^{-1}$ with Pt/γ-Al_2O_3, and at W/F = 0.1 g_{cat} h $g_{cresol}{}^{-1}$ with Pt/SiO_2 and Pt/Na-B catalysts. The conditions were chosen in order to observe deactivation. After 3 h of reaction, the catalysts were purged for 30 min in H_2 and then 30 min in N_2. Afterwards the catalysts were treated 1 h in air at 350 °C, activated 1 h in H_2 and a new reaction cycle was carried out. Alternatively, a treatment in H_2 at 500 °C, instead of air, was used for catalyst regeneration.

3. Results and discussion

3.1. Catalysts characterization

3.1.1. BET surface and pores characterization

Table 1 shows the results of surface characterization. The Pt/γ-Al_2O_3 catalyst is a typical mesoporous catalyst, while the Pt/SiO_2 presents both, micro and small mesopores. Also, the H-B and modified H-B catalysts, as well as these materials impregnated with platinum, contain both micro and mesopores. The mesopores distribution of all these catalysts is wide, with pores sizes between 20 and 300 Å, but the distribution profiles are similar for all of them.

The adsorption–desorption isotherm (not shown) for the H-B presents a non pronounced hysteresis loop, which indicates that there is an important contribution of the external surface to the relatively high value of mesoporous area. The micropore volume of 0.19 cm^3 g^{-1} is typical for the BEA framework [29]. The alkaline treatment of H-B with NaOH to obtain Na-B did not produce significant changes in the isotherm, decreasing slightly the micropore volume, but did not modify the mesopores volume. Also, as will be shown below, there was not a significant change in the crystallinity degree. J. Groen et al. [30] studied the desilication of a Beta zeolite (Si/Al = 35) with a 0.2 M NaOH solution, at 338 K for 30 min, employing 30 ml of solution per gram of zeolite, achieving mesoporous formation. It was found that the micropore volume and crystallinity of the alkaline-treated beta was severely diminished. On the other hand, in the present work, the amount of alkaline solution used per gram of catalyst was much lower, 10 ml g^{-1}, with the aim of exchanging the protons of the H-B zeolite. Then, the main difference between the H-B and the Na-B was the acid property, as will be shown below, maintaining a similar pore structure.

3.1.2. Crystalline structure and platinum dispersion

The X-ray diffractograms of the Pt/γ-Al_2O_3 catalyst (not shown) presents the typical signals of the γ-Al_2O_3 at 2θ = 45.901, 67.093,

Table 1
Surface characterization.

Catalyst	Total surface area ($m^2\ g^{-1}$)	Microp. surface area ($m^2\ g^{-1}$)	Mesop. surface area ($m^2\ g^{-1}$)	Microp. volume ($cm^3\ g^{-1}$)	Mesop. volume ($cm^3\ g^{-1}$)	Total pores volume ($cm^3\ g^{-1}$)
Pt/γ-Al_2O_3	214	5	209	0.004	0.48	0.49
Pt/SiO_2	359	57	302	0.025	1.44	1.47
H-B	699	372	327[b]	0.19	0.36	0.55
LCH-B	605	320	285[b]	0.16	0.34	0.50
LCL-B	626	350	276[b]	0.18	0.33	0.51
Na-B	593	333	260[b]	0.17	0.35	0.52
Pt/H-B	487	294	193[b]	0.15	0.21	0.36
Pt/Na-B	506	303	203[b]	0.15	0.28	0.43
Pt/Na-B used[a]	85	38	47[b]	0.02	0.07	0.09

[a] Reaction conditions: 6.5 h, W/F = 0.15 g_{cat} h. g_{cresol}^{-1}, H_2/m-cresol molar ratio = 65. Final conversion value: 33%.
[b] Mesoporous assigned to external surface area contributions.

Table 2
Metallic dispersions obtained by hydrogen and carbon monoxide chemisorption and metal sites/acid sites ratio (MS/AS) for fresh catalysts.

Catalyst	H_2-dispersion (%)	CO-dispersion (%)	MS/AS ratio 10^2
Pt/γ-Al_2O_3	21.7	nm	189.2
Pt/SiO_2	25.0	28.4	183.0
Pt/H-B	nm	12.3	2.7
Pt/LCH-B	nm	21.4	4.3
Pt/LCL-B	nm	28.2	9.2
Pt/Na-B	19.6	18.5	3.1
Pt/NaH-B	19.1	nm	2.7

nm: not measured.

37.635, 39.524, and 19.466 (JCPDS-ICDD 10-425). No signals of Pt were observed (JCPDS-ICDD 4-802) since the particles were small enough due to its high dispersion. In the Pt/SiO_2 diffractogram (not shown) only an amorphous halo was observed, having a characteristic peak at $2\theta = 23.8°$. The metallic dispersions calculated by H_2 and CO chemisorptions are shown in Table 2. The average particle size of Pt was 1.2 nm and 1.7 nm for the Pt/γ-Al_2O_3 and Pt/SiO_2 catalysts, respectively, as determined by TEM. Fig. 1 shows the diffractograms of the fresh zeolites-based catalysts, and indicate that the zeolitic structure was preserved upon the exchange treatment either with lanthanum or sodium. The XRD spectrum that corresponds to the H-B catalyst (sample a) is the typical for this material. The exchange of protons with lanthanum up to different degrees (samples b and c) did not significantly modify the crystallographic structure, showing only a minor decrease in the intensity of the diffraction peak at 8°. The crystallinity degree of these samples was 93%, taking 100% for the original H-B zeolite. The same result was observed after the ionic exchange with sodium (sample d). The crystallinity degree of all the zeolites after Pt impregnation was 90% (samples e, f, g, h). The Pt signals were observed after impregnation on the different zeolites (Fig. 1), except for the Pt/HB. The Pt crystallite size was calculated using the Scherrer's equation. These values were between 19 and 20 nm for these catalysts.

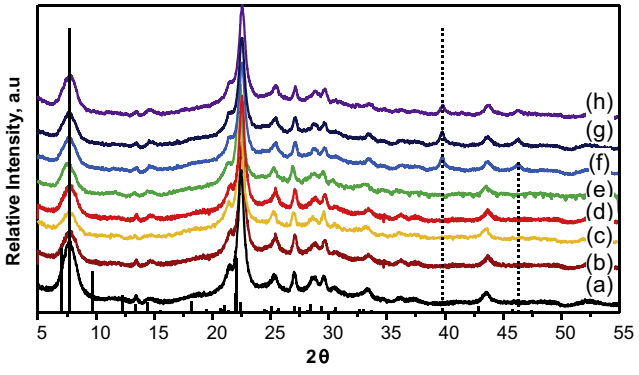

Fig. 1. XRD patterns of fresh Zeolites: (a) H-B, (b) LCH-B, (c) LCL-B and (d) Na-B. Pt/Zeolites: (e) Pt/H-B, (f) Pt/LCH-B, (g) Pt/LCL-B and (h) Pt/Na-B. JCPDS-ICDD characteristic signals for Pt (dash line) and characteristic signals for H-B (solid line).

3.1.3. Platinum reducibility

The Pt/γ-Al_2O_3 TPR profile (not shown) presented two peaks, one at 240 °C and the second at 414 °C, which can be assigned to the bulk phase of the PtO_x and to highly dispersed particles with strong interaction with the support, respectively, as previously reported [31–33]. These two peaks for Pt/SiO_2 were at 127 and 404 °C, for Pt/H-B at 114 and 506 °C, and for Pt/Na-B at 100 and 485 °C. According to these results, all the catalysts were activated at 500 °C in H_2 stream for 1 h.

3.1.4. Total acidity and acid sites strength distribution

Acid sites density and strength distribution were obtained by Py-TPD analyses. Results are shown in Figs. 2 and 3. The TPD profiles shown in Fig. 2 correspond to Pt/γ-Al_2O_3, Pt/SiO_2, NaH-B and Pt/NaH-B. Fig. 3 shows the profiles for the zeolites H-B, LCH-B, LCL-B and Na-B without Pt. The impregnation of 1.7 wt% of Pt on NaH-B zeolite did not modify the shape of the TPD profile, but the acid sites density increased (compare Fig. 2C and D). This might be due to the fact that the precursor solution was slightly acid (pH = 6). The values of the total acid sites densities obtained by Py-TPD, are summarized in Table 3. As it is well known Pt/γ-Al_2O_3 and Pt/SiO_2 have a very low total acid sites density in comparison with the zeolites. The profiles deconvolution identifies three different desorption peaks of pyridine at low-temperature, medium-temperature and high-temperature regions, thus suggesting the presence of acid sites with different strengths, weak (w), medium (m) and strong (s), respectively. The Pt/γ-Al_2O_3 has mostly medium and strong acid sites, and the Pt/SiO_2 catalyst has mainly weak acid sites. Moreover, the zeolites have a broader acid strength distribution. Esquivel et al. [34] observed a similar TPD profile for the H-BEA catalyst. Fig. 3B shows that the incorporation of lanthanum into the zeolite structure led to changes in the distribution of acid sites strength, increasing the proportion of the sites from which the pyridine desorbed in the medium-temperature range, approximately at 410 °C (compare with Fig. 3A). The protonic form of Beta zeolite has similar amount of medium and high strength acid sites, as shown in Fig. 3A and Table 3, while the catalyst partially exchanged with lanthanum (LCH-B) has mostly medium-strength acid sites (Fig. 3B, Table 3). The acid sites density decreased in the order H-B ≈ LCH-B > LCL-B. The exchange with sodium also modified the Py-TPD profile, increasing the total acid sites density and the proportion of weak acid sites in the Na-B zeolite compared to the protonic form (compare Fig. 3A and D, also see Table 3). These observations revealed that Brønsted acid sites of medium-strong were those

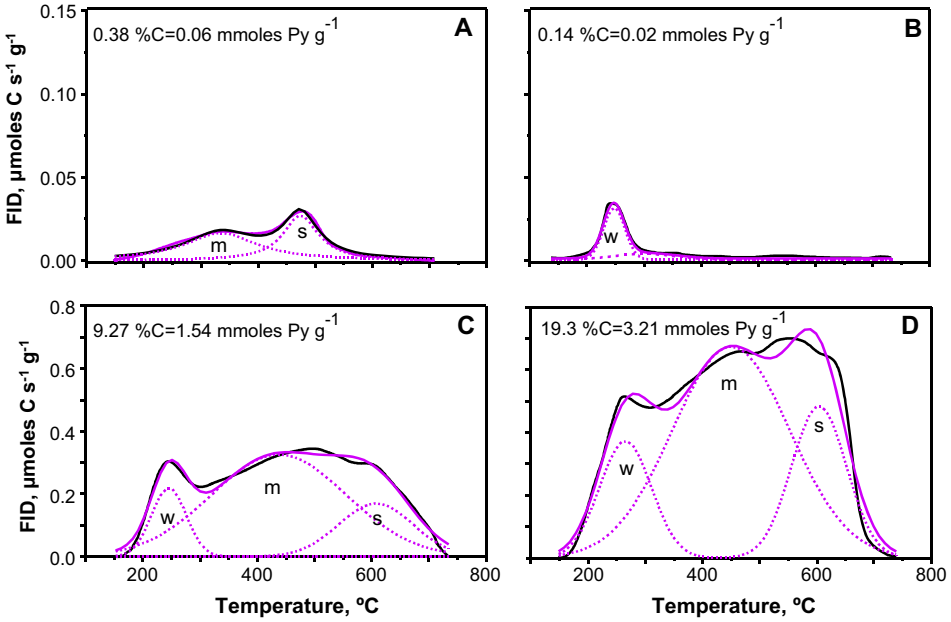

Fig. 2. Pyridine TPD profiles of fresh catalysts after reduction: (A) Pt/γ-Al_2O_3, (B) Pt/SiO_2, (C) NaH-B, (D) Pt/NaH-B. Weak (w), medium (m) and strong (s) acid sites.

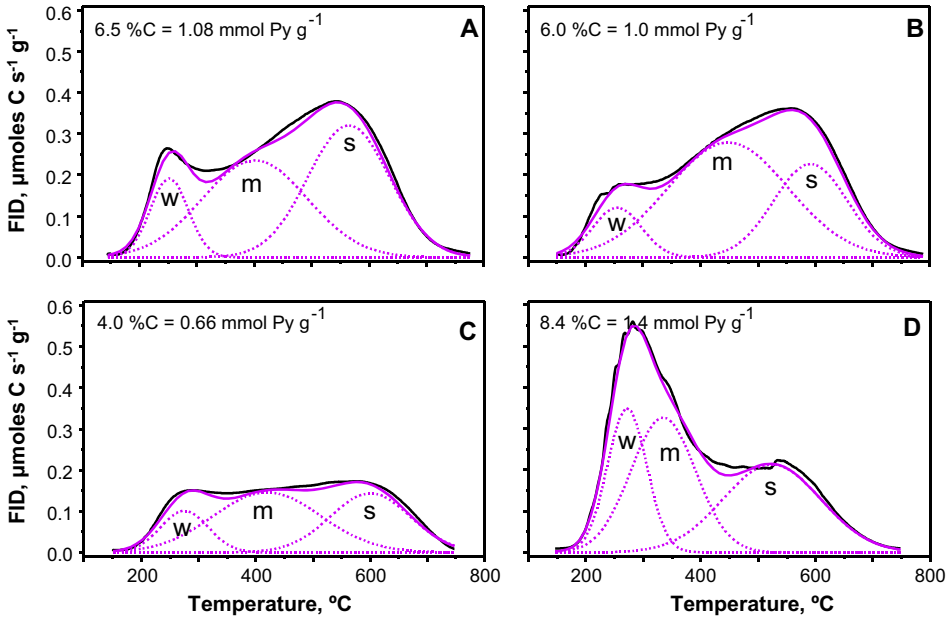

Fig. 3. Pyridine TPD profiles of fresh zeolites: (A) H-B, (B) LCH-B, (C) LCL-B and (D) Na-B. Weak (w), medium (m) and strong (s) acid sites.

Table 3
Acid sites densities obtained by Py-TPD.

Catalyst	Total acid sites density (μmol Py m^{-2})	Weak acid sites density (μmol Py m^{-2})	Medium acid sites density (μmol Py m^{-2})	Strong acid sites density (μmol Py m^{-2})
Pt/γ-Al_2O_3	0.296	0.001	0.140	0.155
Pt/SiO_2	0.061	0.043	0.014	0.004
NaH-B	2.153	0.269	0.914	0.970
Pt/NaH-B	5.149	0.609	3.526	1.014
H-B	1.545	0.186	0.658	0.701
LCH-B	1.651	0.165	0.991	0.495
LCL-B	1.053	0.159	0.511	0.383
Na-B	2.360	0.590	0.897	0.873

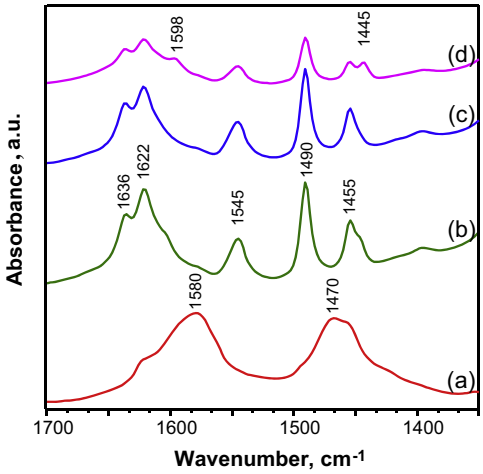

Fig. 4. Pyridine IR profiles after desorption at 250 °C for (a) Pt/γ-Al_2O_3, (b) Pt/H-B, (c) Pt/LCH-B, (d) Pt/Na-B.

preferably exchanged by alkali cations, decreasing their quantity. It was reported that, even in neutral zeolites, piridine-Na interaction exists as the cations are electron acceptors acting as Lewis acid sites [35]. By adding small amounts of water these sites should become Brønsted but, according to J. Rabo [35] this change did not occur, indicating that the acidity observed was more related to pyridine–Na interactions than to a real Lewis acidity. Esquivel et al. [34] also suggested that the exchanged alkaline cations act as acid sites of Lewis nature, able to coordinate molecules of pyridine that desorbs at low temperatures.

3.1.5. FTIR analyses of adsorbed pyridine

The signals associated to chemically adsorbed pyridine appear in the IR spectrum in the range 1700–1400 cm^{-1}. Fig. 4 shows the results of FTIR analyses of adsorbed pyridine on several catalysts. Pyridine adsorbed on Pt/H-B resulted in the appearance of bands at 1622 and 1455 cm^{-1} characteristic of pyridine adsorbed on Lewis acid sites (PyL), at approximately 1545 and 1636 cm^{-1} (PyH^+) that corresponds to pyridine adsorbed on Brønsted acid sites, and the bands attributed to pyridine adsorbed on both Brønsted and Lewis acid sites at 1490 cm^{-1}. The Pt/H-B, Pt/LCH-B and Pt/Na-B present similar Py-IR spectrum, except for the signals at 1598 and 1445 cm^{-1} only present in the Pt/Na-B spectrum. According to Parry [36] these signals are characteristic of Lewis-coordinated pyridine, and might be related to the increased proportion of weak/medium-strong acid sites found in the Na-B catalyst by the Py-TPD analyses, compared to the H-B catalyst (see Table 3). Similar observations were obtained with Na-modified H-ZSM-5 catalysts [32].

The Pt/γ-Al_2O_3 catalyst present only signals corresponding to Lewis acidity, at 1580 and 1470 cm^{-1}, due to the structural properties of this material [37,38]. The Al_2O_3 does not possess Brønsted acid sites.

The Pt/SiO_2 catalyst did not showed any IR signals corresponding to Brønsted or Lewis acidity, although some acidity was detected by Py-TPD, as shown in Fig. 2. This means that the acid sites present on this catalyst are weak enough in order that the pyridine desorbs during the evacuation at 250 °C in vacuum, before the IR measurement.

Pt/γ-Al_2O_3 has mostly strong Lewis acid sites, Pt/SiO_2 has weak acid sites, and Pt/H-B catalysts have Brønsted and Lewis acid sites of different strength. The exchange of H-B with lanthanum or sodium changes its acid strength profile, increasing the proportion of medium to strong acid sites when exchanging with lanthanum, and the proportion of weak to medium + strong acid sites with sodium.

3.2. Influence of acid type, density and strength on product distribution

The reaction scheme for m-cresol deoxygenation using Pt/γ-Al_2O_3 previously proposed [27] is shown in Fig. 5. The main reaction products were toluene, benzene, methylcyclohexane, and light hydrocarbons including mainly methane, ethane, propane, butane, and small amounts of n-pentane, isopentane, 2 and 3 methylhexane and hexane. Phenol was found in very low amounts.

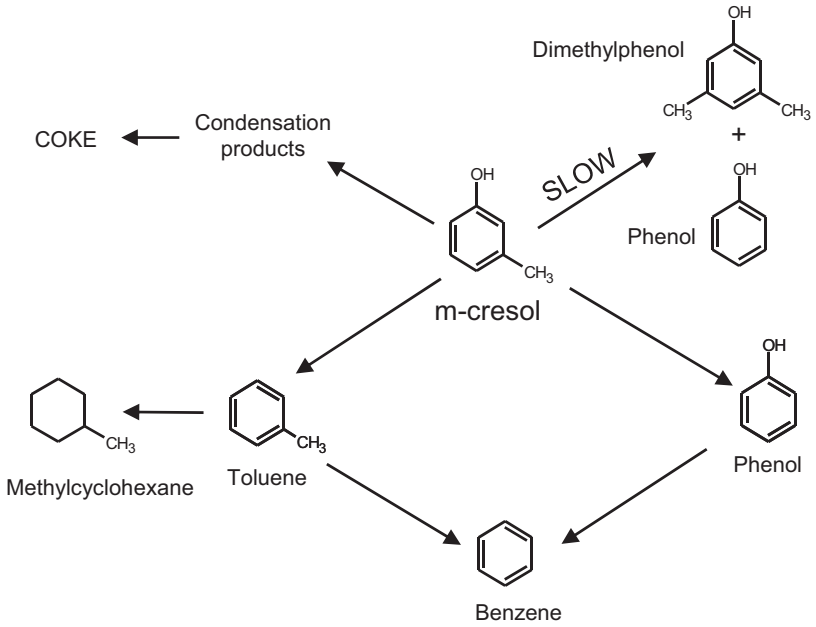

Fig. 5. Reaction scheme for m-cresol deoxygenation.

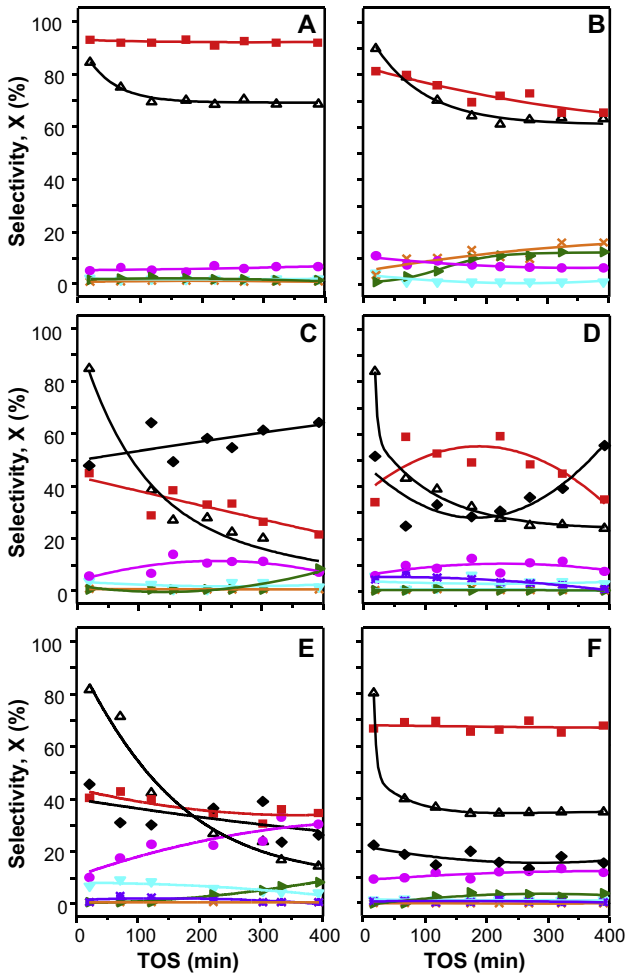

Fig. 6. Cresol conversion and product selectivity vs. time on stream for different catalysts at 300 °C, H_2/m-cresol molar ratio = 65. (A) Pt/γ-Al_2O_3 W/F = 0.1 g_{cat} h g_{cresol}^{-1}, (B) Pt/SiO_2 W/F = 0.24 g_{cat} h g_{cresol}^{-1}, (C) Pt/H-B W/F = 0.1 g_{cat} h g_{cresol}^{-1}, (D) Pt/LCH-B W/F = 0.15 g_{cat} h g_{cresol}^{-1}, (E) Pt/LCL-B W/F = 0.1 g_{cat} h g_{cresol}^{-1}, and (F) Pt/Na-B W/F = 0.15 g_{cat} h g_{cresol}^{-1}. References: (△) m-cresol conversion, (■) toluene, (X) LH, (▼) benzene, (▶) phenol, (●) methylcyclohexane, (✳) xilenes and (♦) heavies. (For interpretation of the references to color in this figure legend, the reader is referred to the web version of this article.)

Toluene is formed by deoxygenation of cresol. It has been proposed that this reaction occurs on the metal after the aromatic ring is partially hydrogenated, and then the C–O bond breakage occurs followed by dehydrogenation of the ring [33]. Phenol is formed by hydrogenolysis of the methyl group of cresol. Two different routes generate benzene: (i) the hydrogenolysis of the methyl group of toluene produces benzene and methane; (ii) the deoxygenation of phenol forms benzene. Methylcyclohexane was formed by hydrogenation of toluene. Other products found by GC–MS in low amounts were dimethyl diphenyl and dimethyl benzophenone. Methyl groups from these compounds can be hydrocracked, and because of this, the light hydrocarbon fraction (which contained an important amount of methane) yield was higher than the benzene yield.

In this work, the product distribution was compared among catalysts containing Pt supported on H-B, LCH-B, LCL-B and Na-B zeolites, and γ-Al_2O_3 and SiO_2. The reaction products were almost the same for all the catalysts, toluene being the main product of deoxygenation, as seen in Fig. 6. It has been shown that a high metal sites/acid sites ratio (MS/AS), as the one that has the Pt/γ-Al_2O_3 catalyst used in this work, favoured the cresol deoxygenation reaction to toluene, while lower values of this ratio favoured the formation of light products, which resulted from cracking of heavy products formed by condensation on the support acid sites. Thus, a high ratio is desired in order to avoid light products formation. Table 2 shows this parameter for all the catalysts used in this study. Fig. 6 also shows that benzene yield was negligible for these reaction conditions, as also reported in the case of Pt/γ-Al_2O_3 catalysts [27]. This is because in the case of this catalyst, benzene was mainly formed by deoxygenation of phenol, being the phenol formation rate much slower than the cresol deoxygenation rate forming toluene. As observed in Fig. 6, the toluene selectivities at TOS = 0 are low for the Pt/zeolites (Fig. 6C–F) and high for the Pt/γ-Al_2O_3 and Pt/SiO_2 catalysts (Fig. 6A and B). This is due to the fact that higher yield to heavy products were obtained with the Pt/zeolites catalysts, as observed in Fig. 6. This difference in the product distribution between the catalysts supported on zeolites and those supported on alumina and silica can be explained in terms of differences in acidity. As observed in Fig. 6, the toluene selectivities were around 40–50% for the Pt/H-B, Pt/LCH-B and Pt/LCL-B catalysts, and approximately 65% for the Pt/Na-B catalyst. As seen in Table 4 the Pt/Na-B catalyst has the lowest density of Brønsted acid sites, which according to these results might be responsible for the production of heavy products. The concentration of Lewis acid sites in the Pt/Na-B catalyst is also the lowest among the zeolites. A major difference between the zeolites and the alumina and silica catalysts is that the acid sites density is approximately one order of magnitude higher in the former. This high density of acid sites favours the formation of condensation products, thus increasing the relative rate of heavy products formation. Another very interesting observation is that among the zeolites, the MS/AS ratio for Pt/Na-B catalyst is an intermediate value, being higher for some of the other Pt/zeolites catalysts (Table 4). However, the toluene yield obtained with Pt/Na-B was the highest among the zeolite-supported catalysts. This means that when the MS/AS ratio is similar, the other parameters above discussed, such as acid sites strength, density and type (Brønsted or Lewis) are relevant to define the selectivity and stability.

Table 4
Acid values obtained by Py-FTIR. Brønsted and Lewis concentrations determined by the 1545 cm^{-1} and 1455 cm^{-1} signals respectively.

Catalyst	Br sites (mmol g^{-1})	Le sites (mmol g^{-1})	Br + Le (mmol g^{-1})	Br/Le ratio
Pt/H-B	0.62	0.33	0.95	1.86
Pt/LCH-B	0.59	0.35	0.94	1.67
Pt/Na-B	0.24	0.13	0.37	1.88
Pt/NaH-B	0.52	0.30	0.82	1.72

In presence of zeolites catalyst xylenes were observed as products. Resasco et al. [19] have shown that acidic zeolites are very effective to catalyze the transalkylation of phenolics and other aromatics. Therefore, it can be expected that methyl groups can be transferred to another aromatic molecule instead of forming methane. It have been also established that species trapped on the catalyst surface can subsequently decompose to products such as benzene, toluene or xylene and light hydrocarbons via cracking or hydrogenolysis [39,20]. In our case xylene production, formed by transalkylation, is not favoured at these low values of W/F and hydrogen partial pressure. Benzene, eventually produced by transalkylation when using high W/F and H_2 partial pressure, is less desired than toluene in gasoline, due to environmental restrictions. Finally, the variation of acid strength obtained by ionic exchanged with lanthanum as seen in Fig. 3, did not lead to significant changes in product distribution, as also observed in other reactions [40].

To summarize, in order to have a high yield of a high octane deoxygenated product like toluene, a high density of Brønsted acid sites is not desired since in this case the formation of heavy products

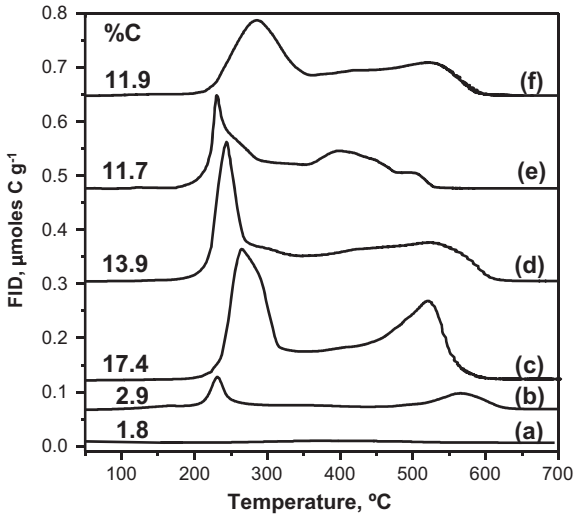

Fig. 7. TPO profiles and coke content for the spent catalysts after 390 min of reaction at 300 °C, H_2/m-cresol molar ratio = 65. References: (a) Pt/γ-Al_2O_3 W/F = 0.1 g_{cat} h g_{cresol}^{-1}, (b) Pt/SiO_2 W/F = 0.24 g_{cat} h g_{cresol}^{-1}, (c) Pt/H-B W/F = 0.1 g_{cat} h g_{cresol}^{-1}, (d) Pt/LCH-B W/F = 0.15 g_{cat} h g_{cresol}^{-1}, (e) Pt/LCL-B W/F = 0.1 g_{cat} h g_{cresol}^{-1}, (f) Pt/Na-B W/F = 0.15 g_{cat} h g_{cresol}^{-1}.

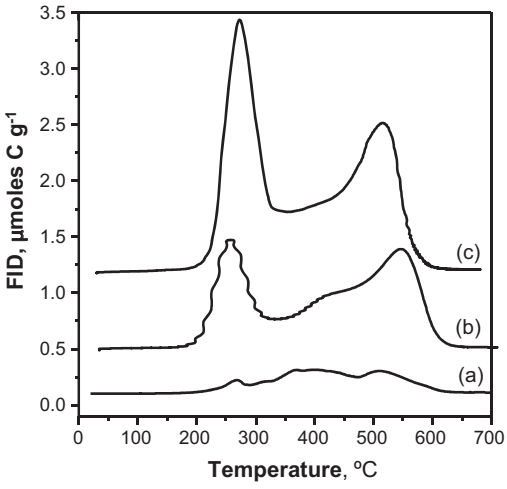

Fig. 8. TPO profiles for the spent Pt/H-B after 390 min of reaction at 300 °C, H_2/m-cresol molar ratio = 65. (a) W/F = 11 g_{cat} h g_{cresol}^{-1}, (b) W/F = 0.5 g_{cat} h g_{cresol}^{-1}; (c) W/F = 0.1 g_{cat} h g_{cresol}^{-1}.

is catalyzed, and therefore, only a relatively small density of acid sites is required, implying a high metal sites/acid sites ratio.

3.3. *Influence of acidity and surface structure in catalyst stability*

All the catalysts studied in this work showed deactivation. Pt/γ-Al_2O_3 and Pt/SiO_2 catalysts achieved the highest values of cresol conversion and toluene selectivity after 400 min of reaction, as observed in Fig. 6. The Pt/γ-Al_2O_3 catalyst reached a pseudo-steady state after 120 min of reaction with values of conversion above 70% and toluene selectivity around 90%. The comparison between Pt/SiO_2 and Pt/γ-Al_2O_3 catalysts shows that, although the total acid sites density is lower in the former, it had a higher accumulation of coke during the reaction, being this amount 2.92% and 1.84% for Pt/SiO_2 and Pt/γ-Al_2O_3 catalysts respectively, as shown in Fig. 7. This is because the acid strength in the Pt/SiO_2 was not enough in order to eliminate the coke precursors from the catalyst surface by hydrocracking. Because of this, it was also possible to observe heavy products in the case of the Pt/SiO_2 catalyst, while they were not obtained with the Pt/γ-Al_2O_3 catalyst. In the last case, the heavy products are hydrocraked leading to the formation of a higher amount of light products (Fig. 6). In addition to the lower acid strength and density of the silica supported catalyst, the presence of Brønsted acid sites, in contrast with Lewis acid sites on the alumina supported catalyst, might play a role in the coking mechanism.

Although the exchange with lanthanum (LCL-B) produced a decrease of the acid sites density, mainly in the strong sites, and led to a catalyst having a higher proportion of intermediate strength sites, the activity and stability were practically the same for Pt/H-B, Pt/LCH-B y Pt/LCL-B catalysts (Fig. 6C–E).

The Pt/LCL-B catalyst has lower total acid sites density and also lower strong acid sites density, compared to the Pt/H-B and Pt/LCH-B catalysts. For these reasons, the Pt/LCL-B formed the lowest amount of coke among these three catalysts. H-B support has higher proportion of strong acid sites than the LCH-B, and because of this, higher amount of coke was formed on the former. However, the stabilities of these catalysts were quite similar, reaching values of conversion of approximately 20–30% at 400 min on stream. The reason of this might be that the catalysts were saturated with coke and almost completely deactivated after 400 min of reaction. On the other hand, it can be observed that, although the Pt/Na-B catalyst formed approximately the same amount of coke than the Pt/LCL-B catalyst, it showed higher values of conversion and toluene selectivity, and stabilized after 150 min on oil (Fig. 6).

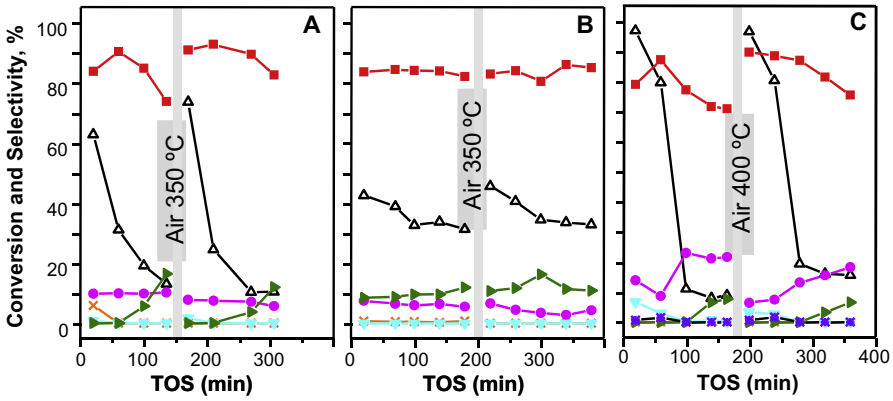

Fig. 9. m-Cresol conversion and product selectivity vs. time on stream at 300 °C, H_2/m-cresol molar ratio = 64, before and after treatment with air for: (A) Pt/γ-Al_2O_3 W/F = 0.08 g_{cat} h g_{cresol}^{-1}, (B) Pt/SiO_2 W/F = 0.1 g_{cat} h g_{cresol}^{-1}, (C) Pt/Na-B W/F = 0.1 g_{cat} h g_{cresol}^{-1}. References: (△) m-cresol conversion; (■) toluene, (X) LH, (▼) benzene, (▶) phenol, (●) methylcyclohexane and (✳) xilenes. (For interpretation of the references to color in this figure legend, the reader is referred to the web version of this article.)

Another fact to consider is that the activity dropped rapidly with Pt/zeolites in contrast with the Pt/γ-Al_2O_3 and Pt/SiO_2 catalysts, due to the fast coke deposition, leading to the formation of more than 10 wt% coke. The BET surface area of Pt/Na-B catalyst decreased importantly after being used in reaction (6.5 h, W/F = 0.15 g_{cat} h g_{cresol}^{-1}, H_2/m-cresol molar ratio = 65), as shown in Table 1. The internal surface area decreased 8 times and the external surface area decreased 4 times, while the micropore volume changed from 0.15 to 0.02 cm^3 g^{-1}. Evidently, the coke deposition that occurred on the Pt/zeolites catalysts led to a pore blocking, and consequently a fast deactivation was observed. The combination of high-density of acid sites and microporous structure is detrimental to the catalyst stability. The amount of carbon deposited on the spent Pt/zeolites after 400 min of reaction was 3 to 6 times higher than the one deposited on Pt/SiO_2 and more than 9 times higher than the one deposited on Pt/γ-Al_2O_3 (Fig. 7). This explains the higher stability, conversion level and toluene selectivity of Pt/γ-Al_2O_3 catalyst.

Experiments at different W/F values with Pt/H-B were carried out. The TPO profiles of spent catalysts are shown in Fig. 8. The two main maxima observed for each profile correspond to carbon deposited on the metal or near the metal particles, and on the support, respectively [41–43]. It can be seen that, for higher residence times (curve a), coke was mainly formed on acid sites (burning at higher temperatures), and for lower contact times coke was deposited on both metallic and acid sites. Thus, the same tendency as that found with Pt/γ-Al_2O_3 catalyst was observed with the Pt/H-B catalysts, confirming that acid sites deactivate faster than metallic sites. It is evident that after the first peak in the TPO profile, there is a small signal with a maximum at approximately 400–450 °C, before a larger peak that was assigned to coke on the support. In fact these two signals are associated to coke on the support, and this separation has been previously demonstrated that are due to coke reorganization, that occurs on the acid sites as the temperature is increased above that used in the reaction [44].

3.4. Coke deposits and catalyst regeneration

Fig. 7 shows the TPO profiles for all the spent catalysts studied in this work. The W/F was between 0.08 and 0.10 g_{cat} h g_{cresol}^{-1} for the different catalysts, and the H_2/m-cresol molar ratio 65 in all cases. The residence time was low enough in order to clearly observe the deactivation/regeneration phenomena. Two maxima at around 250 °C and 530 °C were observed in all the TPO profiles, except for the Pt/γ-Al_2O_3 catalyst, that displayed only the second peak. However, in the case of more deactivated Pt/γ-Al_2O_3 catalyst, these two maxima were also observed [27]. As mentioned before, these two maxima correspond to carbon deposited on the metal or near the metal particles and on the support, respectively. Only in the case of Pt/LCL-B catalyst, the second maximum was shifted to around 400 °C, which was lower than in the other zeolite supported catalysts. Fig. 9 shows cycles of reaction before and after a regeneration treatment with air at 350 °C for Pt/γ-Al_2O_3, Pt/SiO_2, and at 400 °C for Pt/Na-B catalysts. At these conditions the regeneration was feasible

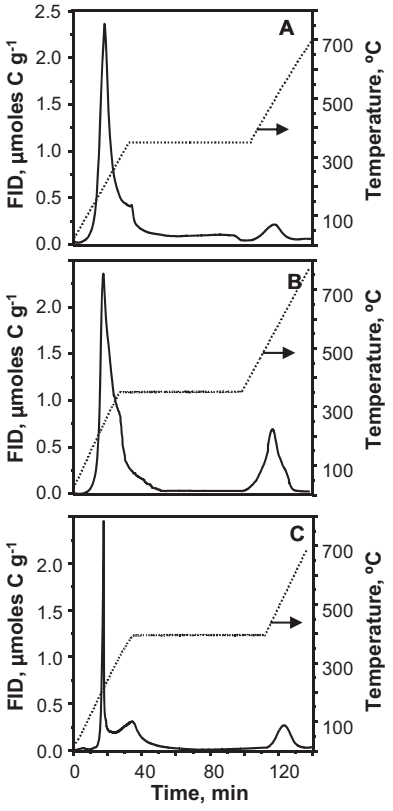

Fig. 10. TPO profiles for the spent catalysts after 160 min of reaction at 300 °C, H_2/m-cresol molar ratio = 64, maintaining 1 h at 350 °C, (A) Pt/γ-Al_2O_3 W/F = 0.08 g_{cat} h g_{cresol}^{-1}, (B) Pt/SiO_2 W/F = 0.1 g_{cat} h g_{cresol}^{-1} and (C) Pt/Na-B W/F = 0.1 g_{cat} h g_{cresol}^{-1}.

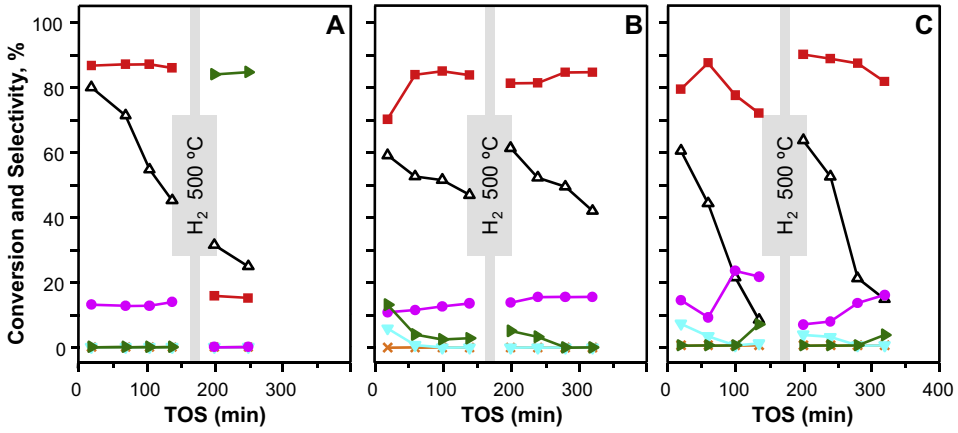

Fig. 11. m-Cresol conversion and product selectivity vs. time on stream at 300 °C, H_2/m-cresol molar ratio = 64, before and after treatment with H_2 at 500 °C for: (A) Pt/γ-Al_2O_3 W/F = 0.08 g_{cat} h g_{cresol}^{-1}, (B) Pt/SiO_2 W/F = 0.15 g_{cat} h g_{cresol}^{-1} and (C) Pt/Na-B W/F = 0.09 g_{cat} h g_{cresol}^{-1}. References: (△) m-cresol conversion, (■) toluene, (X) LH, (▼) benzene, (▶) phenol, and (●) methylcyclohexane. (For interpretation of the references to color in this figure legend, the reader is referred to the web version of this article.)

in the three cases. In order to determine the amount of coke left on the catalysts after the regeneration treatments, samples of coked catalysts were treated during 1 h in air at the regeneration temperature. Then, the temperature was raised in order to determine the amount of coke not eliminated during the regeneration treatment. The results are shown in Fig. 10. A small fraction of the total amount of coke was left on the catalyst during the regeneration, and corresponds to the small peak displayed at approximately 120 min on the TPO profiles shown in Fig, 10. This peak represents 8%, 24%, and 22% for Pt/γ-Al_2O_3, Pt/SiO_2, and Pt/Na-B catalysts respectively.

The low temperature used in the treatment with air was enough to regenerate the catalysts, obtaining the same activity and selectivity in the second cycle compared to the first one. This means that the small proportion of coke that remained on the acid sites after the regeneration treatment was responsible for the slightly higher selectivity to toluene and lower selectivity to heavy products in the second cycle, i.e., as the (metal function/acid function) ratio slightly increased.

In addition to the regeneration treatment in air stream, a treatment in H_2 at 500 °C was carried out with Pt/γ-Al_2O_3, Pt/SiO_2 and Pt/Na-B catalysts. Fig. 11 shows the reactions before and after this treatment. The regeneration was possible with Pt/SiO_2 and Pt/Na-B catalysts, but not with Pt/γ-Al_2O_3. The reason is that the high temperature treatment in hydrogen of Pt/γ-Al_2O_3 catalyst, led to the formation of a coke with high toxicity, decreasing the activity of the acid function in such a way that the catalyst looses the activity for the dehydration step that is needed in order to obtain toluene. This occurred in the case of the Pt/γ-Al_2O_3 and not with the Pt/SiO_2 and Pt/Na-B catalysts because of the higher acid strength of the former.

3.5. Conclusions

The influences of acid sites density, type and strength, as well as surface structure, were analyzed for the cresol deoxygenation reaction at atmospheric pressure with Pt catalysts supported on low and mild acid materials. Toluene, which is a high octane index compound, was the main deoxygenated product for all the catalysts studied. In order to have a high yield of this compound, a high metal sites/acid sites ratio is required to rapidly form toluene avoiding the formation of cracking products. Only a small density of acid sites is required since dehydration is proposed to be one of the steps involved in the cresol deoxygenation reaction. A high density of acid sites is undesirable for catalyst stability, due to coke formation via condensation of precursors adsorbed on adjacent sites. Besides, mesoporous structures are more convenient since on Pt/zeolites the deactivation was faster due to mouth pore blocking. For all these reasons, Pt/γAl_2O_3 and Pt/SiO_2 catalysts, showed a better catalytic behaviour than Pt/H-B and modified Pt/H-B catalysts. In fact, the Pt/γAl_2O_3 catalyst showed the best performance, due to an appropriate combination of metal to acid sites ratio, acid sites strength and density.

The ionic exchange of H-B catalyst with lanthanum modified the strength of the acid sites, decreasing the proportion of strong/medium strength sites. However there is not an appreciable effect of this variable on product distribution. Only the amount of coke formed increased with acid strength, but this was not reflected on catalysts stability at these reaction conditions.

Coke is formed on the metal as well as on the acid sites. The acid sites are poisoned faster than the metallic sites. A treatment in air at 350 °C is enough to regenerate all the catalysts studied here, recovering the metallic sites and a high fraction of the acid sites.

Acknowledgments

The authors wish to acknowledge the financial support received from ANPCyT (PICT 2010-1526), CONICET (PIP 2010-093) and UNL (CAID PACT 069). Thanks are also given to Diego López Delzar, José Ignacio Lobos and Claudio Perezlindo for the technical support, and to Elsa Grimaldi for the English language editing.

References

[1] J. Piskorz, D. Scott, D. Radlein, E. Soltes, T. Milne, ACS Symp. Ser. (1988) 167–178.
[2] C. Amen-Chen, H. Pakdel, C. Roy, Bioresour. Technol. 79 (2001) 277–299.
[3] S. Czernik, A. Bridgwater, Energy Fuels 18 (2004) 590–598.
[4] A. Oasmaa, S. Czernik, Energy Fuels 13 (1999) 914–921.
[5] Y.-H.E. Sheu, R.G. Anthony, E.J. Soltes, Fuel Process. Technol. 19 (1988) 31–50.
[6] E.G. Baker, D.C. Elliott, in: A.V. Bridgwater, J.L. Kuester (Eds.), Research in Thermochemical Biomass Conversion, Springer, Netherlands, 1988, pp. 883–895.
[7] F. Agblevor, S. Besler, Energy Fuels 10 (1996) 293–298.
[8] B. Yoosuk, D. Tumnantong, P. Prasassarakich, Chem. Eng. Sci. 79 (2012) 1–7.
[9] W. Wang, Y. Yang, H. Luo, T. Hu, W. Liu, Catal. Commun. 12 (2011) 436–440.
[10] Y. Romero, F. Richard, Y. Renème, S. Brunet, Appl. Catal. A 353 (2009) 46–53.
[11] E.O. Odebunmi, D.F. Ollis, J. Catal. 80 (1983) 56–64.
[12] R. Kallury, T. Tidwell, D. Boocock, D. Chow, Can. J. Chem. 62 (1984) 2540–2545.
[13] C.R. Lee, J.S. Yoon, Y.-W. Suh, J.-W. Choi, J.-M. Ha, D.J. Suh, Y.-K. Park, Catal. Commun. 17 (2012) 54–58.
[14] B. Yoosuk, D. Tumnantong, P. Prasassarakich, Fuel 91 (2012) 246–252.
[15] V.N. Bui, D. Laurenti, P. Afanasiev, C. Geantet, Appl. Catal. B 101 (2011) 239–245.
[16] Y. Romero, F. Richard, S. Brunet, Appl. Catal. B 98 (2010) 213–223.
[17] V.N. Bui, D. Laurenti, P. Delichère, C. Geantet, Appl. Catal. B 101 (2011) 246–255.
[18] E.-J. Shin, M.A. Keane, Ind. Eng. Chem. Res. 39 (2000) 883–892.
[19] A. Ausavasukhi, Y. Huang, A.T. To, T. Sooknoi, D.E. Resasco, J. Catal. 290 (2012) 90–100.
[20] X. Zhu, L.L. Lobban, R.G. Mallinson, D.E. Resasco, J. Catal. 281 (2011) 21–29.
[21] J. Adjaye, N. Bakhshi, Biomass Bioenergy 8 (1995) 131–149.
[22] P. Chantal, S. Kaliaguine, J. Grandmaison, Appl. Catal. A 18 (1985) 133–145.
[23] A.G. Gayubo, A.T. Aguayo, A. Atutxa, R. Aguado, J. Bilbao, Ind. Eng. Chem. Res. 43 (2004) 2610–2618.
[24] R. Olcese, M. Bettahar, D. Petitjean, B. Malaman, F. Giovanella, A. Dufour, Appl. Catal. B 115 (2012) 63–73.
[25] M.A.n. González-Borja, D.E. Resasco, Energy Fuels 25 (2011) 4155–4162.
[26] J. Filley, C. Roth, J. Mol. Catal. A 139 (1999) 245–252.
[27] M.S. Zanuttini, C.D. Lago, C.A. Querini, M.A. Peralta, Catal. Today 213 (2013) 9–17.
[28] J. Benson, H. Hwang, M. Boudart, J. Catal. 30 (1973) 146–153.
[29] C. Baerlocher, L.B. McCusker, D.H. Olson, Atlas of Zeolite Framework Types, E-Publishing, Elsevier, Amsterdam, 2007.
[30] J.C. Groen, S. Abelló, L.A. Villaescusa, J. Pérez-Ramírez, Microporous Mesoporous Mater. 114 (2008) 93–102.
[31] C. Meephoka, C. Chaisuk, P. Samparnpiboon, P. Praserthdam, Catal. Commun. 9 (2008) 546–550.
[32] M.J. Tiernan, O.E. Finlayson, Appl. Catal. B 19 (1998) 23–35.
[33] A.C.S.F. Santos, S. Damyanova, G.N.R. Teixeira, L.V. Mattos, F.B. Noronha, F.B. Passos, J.M.C. Bueno, Appl. Catal. A 290 (2005) 123–132.
[34] D. Esquivel, A.J. Cruz-Cabeza, C. Jiménez-Sanchidrián, F.J. Romero-Salguero, Microporous Mesoporous Mater. 142 (2011) 672–679.
[35] J.A. Rabo, Zeolite Chemistry and Catalysis, Am. Chem. Soc., Washington, DC, 1976.
[36] E.P. Parry, J. Catal. 2 (1964) 371–379.
[37] M. Guzman-Castillo, F. Hernández-Beltrán, J. Fripiat, A. Rodriquez-Hernández, R. León, J. Navarrete-Bolaños, A. Tobón-Cervantes, X. Bokhimi, Catal. Today 107 (2005) 874–878.
[38] M. Zaki, M. Hasan, L. Pasupulety, Langmuir 17 (2001) 768–774.
[39] X. Zhu, R.G. Mallinson, D.E. Resasco, Appl. Catal. A 379 (2010) 172–181.
[40] B. Dalla Costa, M.A. Peralta, C.A. Querini, Appl. Catal. A 472 (2014) 53–63.
[41] J. Barbier, E. Churin, P. Marecot, J. Catal. 126 (1990) 228–234.
[42] J. Barbier, in: B. Delmon, G.F. Froment (Eds.), Studies in Surface Science and Catalysis, Elsevier, Amsterdam, 1987, pp. 1–19.
[43] J. Barbier, E. Churin, J. Parera, J. Riviere, React. Kinet. Catal. Lett. 29 (1985) 323–330.
[44] C.A. Querini, E. Roa, Appl. Catal. A 163 (1997) 199–215.